Comptes Rendus

Physique

Luis Enrique Parra López, Loïc Moczko, Joanna Wolff, Aditya Singh, Etienne Lorchat, Michelangelo Romeo, Takashi Taniguchi, Kenji Watanabe and Stéphane Berciaud

Single- and narrow-line photoluminescence in a boron nitride-supported MoSe₂/graphene heterostructure

Recent advances in 2D material physics / *Physique des matériaux bidimensionnels*

Single- and narrow-line photoluminescence in a boron nitride-supported MoSe$_2$/graphene heterostructure

Luis Enrique Parra López[a]**, Loïc Moczko**[a]**, Joanna Wolff**[a]**, Aditya Singh**[a, b]**,
Etienne Lorchat**[a]**, Michelangelo Romeo**[a]**, Takashi Taniguchi**[c]**,
Kenji Watanabe**[d]** and Stéphane Berciaud**⊕ *, [a, e]

[a] Université de Strasbourg, CNRS, Institut de Physique et Chimie des Matériaux de Strasbourg (IPCMS), UMR 7504, F-67000 Strasbourg, France

[b] Department of Physics, Indian Institute of Technology Delhi, 110016, New Delhi, India

[c] International Center for Materials Nanoarchitectonics, National Institute for Materials Science, 1-1 Namiki, Tsukuba 305-0044, Japan

[d] Research Center for Functional Materials, National Institute for Materials Science, 1-1 Namiki, Tsukuba 305-0044, Japan

[e] Institut Universitaire de France, 1 rue Descartes, 75231 Paris cedex 05, France

E-mails: luis.parralopez@ipcms.unistra.fr (L. E. Parra López),
loic.moczko@ipcms.unistra.fr (L. Moczko), joanna.wolff@etu.unistra.fr (J. Wolff),
phz168205@iitd.ac.in (A. Singh), etienne.lorchat@gmail.com (E. Lorchat),
michelangelo.romeo@ipcms.unistra.fr (M. Romeo), taniguchi.takashi@nims.go.jp
(T. Taniguchi), WATANABE.Kenji.AML@nims.go.jp (K. Watanabe),
stephane.berciaud@ipcms.unistra.fr (S. Berciaud)

Abstract. Heterostructures made from van der Waals (vdW) materials provide a template to investigate a wealth of proximity effects at atomically sharp two-dimensional (2D) heterointerfaces. In particular, near-field charge and energy transfer in vdW heterostructures made from semiconducting transition metal dichalcogenides (TMD) have recently attracted interest to design model 2D "donor–acceptor" systems and new optoelectronic components. Here, using Raman scattering and photoluminescence spectroscopies, we report a comprehensive characterization of a molybedenum diselenide (MoSe$_2$) monolayer deposited onto hexagonal boron nitride (hBN) and capped by mono- and bilayer graphene. Along with the atomically flat hBN susbstrate, a single graphene epilayer is sufficient to passivate the MoSe$_2$ layer and provides a homogenous environment without the need for an extra capping layer. As a result, we do not observe photo-induced doping in our heterostructure and the MoSe$_2$ excitonic linewidth gets as narrow as 1.6 meV, approaching the homogeneous limit. The semi-metallic graphene layer neutralizes the 2D semiconductor and enables picosecond non-radiative energy transfer that quenches radiative recombination from long-lived states. Hence, emission from the neutral band edge exciton largely dominates the photoluminescence spectrum of the

---

* Corresponding author.

$MoSe_2$/graphene heterostructure. Since this exciton has a picosecond radiative lifetime at low temperature, comparable with the non-radiative transfer time, its low-temperature photoluminescence is only quenched by a factor of 3.3 ± 1 and 4.4 ± 1 in the presence of mono- and bilayer graphene, respectively. Finally, while our bare $MoSe_2$ on hBN exhibits negligible valley polarization at low temperature and under near-resonant excitation, we show that interfacing $MoSe_2$ with graphene yields a single-line emitter with degrees of valley polarization and coherence up to ~ 15 %.

1. Introduction

Semiconducting transition metal dichalcogenides (TMDs) are layered crystals that exhibit a unique set of optical and electronic properties. In particular, TMDs undergo an indirect-to-direct bandgap transition when thinned down to the monolayer limit [1,2]. Enhanced Coulomb interactions combined with reduced dielectric screening in two dimensions endow mono and few-layer TMDs with room-temperature stable excitonic manifolds [3, 4]. In addition, TMD monolayers possess a valley pseudo-spin degree of freedom that can be manipulated using schemes inspired by decades of developments in optically-controlled spin dynamics [5, 6]. Moreover, the relatively easy isolation of TMD monolayers layers and their stacking with partner layered materials in van der Waals (vdW) heterostructures offer opportunities to tune their properties and discover new electronic and optical phenomena [7], as well as new proximity effects [8, 9] at atomically-sharp heterointerfaces. These fundamental properties can potentially be harnessed for an emerging generation of optoelectronic [7, 10] and valleytronic systems [11, 12].

A pivotal example are TMD/graphene vdW heterostructures. Indeed, combining the semi-metallic and optically transparent character of graphene [13, 14] with the unique optical properties of TMDs [3] yields a platform for light-emitting systems which, as opposed to bare TMD monolayers, retain a high degree of valley polarization and, importantly, of valley coherence up to room temperature [15]. The reason is that there is an efficient non-radiative transfer of photoexcited carriers and excitons from the TMD to graphene [16–19]. This coupling shortens the excitonic lifetime down to the picosecond range and may thus significantly quench photoluminescence (PL), in particular at room temperature [16–18], where the effective excitonic lifetime of a bare TMD monolayer can exceed one nanosecond [17]. An interesting situation arises at low temperature, where the radiative lifetime of the neutral exciton [20, 21] is of the same order as the exciton transfer time towards graphene [22]. In this case, neutral exciton emission is minimally quenched. In contrast, non-radiative transfer remains sufficiently fast to massively quench emission from all the other long-lived excitonic species (including charged excitons, spin-dark excitons, localized excitons, exciton-phonon replica, ... [3]). Moreover, since the Dirac point of graphene lies within the bandgap of Mo- and W-based TMDs, the graphene layer acts as a broadband acceptor of electrons and holes for moderate doping levels below ~10^{13} cm^{-2} [23–25], resulting in a complete neutralization of the TMD *in the dark* through static charge transfer [26]. The combination of these two filtering effects produces single-line PL spectra arising from the radiative recombination of neutral excitons [22].

Beyond these general considerations, the photophysics of 2D materials and a fortiori of TMD/graphene heterostructures subtly depends on extrinsic factors and it is therefore necessary to carefully control their local chemical and dielectric environment. For instance, investigations in high vacuum prevents physisorption of water and organic molecules. Besides, it is known that conventional transparent susbtrates such as SiO_2 can host trapped charges and

favor photoinduced doping [17, 27–29]. A workaround is to use a more inert material such as hexagonal boron nitride (hBN). Indeed, hBN has proven to be an invaluable vdW material ever since its introduction as a dielectric substrate to reveal the intrinsic electron transport properties of graphene [30]. Its atomically flat nature and optical transparency provides a smooth, homogeneous environment that preserves the intrinsic optical features of TMDs. A direct manifestation is the narrowing of the emission lines in hBN-capped samples [31, 32], with linewidths near 1 meV that approach the homogeneous limit at cryogenic temperatures [21, 33–35].

In this paper, using a combination of PL and Raman spectroscopies, we investigate an hBN-supported $MoSe_2$ monolayer capped by a graphene flake containing monolayer (1LG) and bilayer domains (2LG). We show that this minimal vdW assembly benefits both from the capping properties of hBN and from the emission filtering effect of graphene, leading to the absence of photoinduced doping combined with single-line intrinsic excitonic emission with linewidths as low as 1.6 meV at 14 K. In addition, we measure finite degrees of valley polarization and, importantly, of valley coherence up to ~15% at cryogenic temperatures. These results are promising considering the particularly small valley contrasts reported in $MoSe_2$ samples [36, 37].

2. Optical characterization at room temperature

Figure 1(a) shows an optical image of our hBN-supported $MoSe_2$/graphene sample deposited onto a Si/SiO_2 substrate. The side view of the $hBN/MoSe_2$ and $hBN/MoSe_2$/1LG are sketched in Figure 1(b) and typical room temperature PL spectra these two systems are shown in Figure 1(c). The main PL peak slightly below 1.6 eV arises from the recombination of the lowest lying optically active $MoSe_2$ exciton (X^0, also known as the A-exciton) possibly with a minor contribution coming from the trion (charged exciton, X^*) [38]. The photophysics of this heterostructure is driven by the efficient energy transfer from the thermalized excitonic population towards the graphene layer, leading to strong PL quenching by about two orders of magnitude (see scaling factor in Figure 1(c)). As an indirect consequence of the picosecond lifetime of the band-edge exciton, we observe a broad, high energy shoulder on the $MoSe_2$/1LG PL spectrum that is assigned to hot luminescence from excited excitonic states, including Rydberg-like states from from the A-exciton manifold as well as the B-exciton (located near 190 meV above the band-edge A-exciton) [17]. No sizeable hot PL signal is detected in the linear regime in the hBN-supported $MoSe_2$ reference.

We now investigate the possibility of photoinduced charge transfer (i.e., photodoping) in the $hBN/MoSe_2$/1LG region of our sample. As indicated above, band offsets between TMD and graphene allow electron and hole transfer from the TMD to graphene. Besides this intrinsic phenomenon, the presence of surface traps and molecular adsorbates (either on the substrate or on the 2D material) [27, 28], as well as chalcogen vacancies and other local defects in TMDs [39] can facilitate charge transfer and alter exciton dynamics. Under light illumination above the TMD bandgap, a net photoinduced charge transfer to graphene has been observed on SiO_2-supported samples on timescales that are orders of magnitude longer than the TMD excitonic lifetime, hence with no sizeable effect on the PL intensity [17, 40, 41]. This photodoping leads to a stationary Fermi level shift in graphene and complementary fingerprints of charge transfer in the TMD monolayer [17, 29]. The Fermi level of graphene ultimately saturates as the photon flux increases [17, 29]. Although such extrinsic effects could be of practical use for photodetection [40, 41], they may hamper access to the intrinsic photophysics of the heterostructure. In our sample, the bottom hBN flake provides a flat substrate that passivates the $MoSe_2$/graphene heterostructure and could minimize extrinsic photodoping. Quantitative insights into photodoping can be obtained using micro-Raman spectroscopy [42] of the graphene flake.
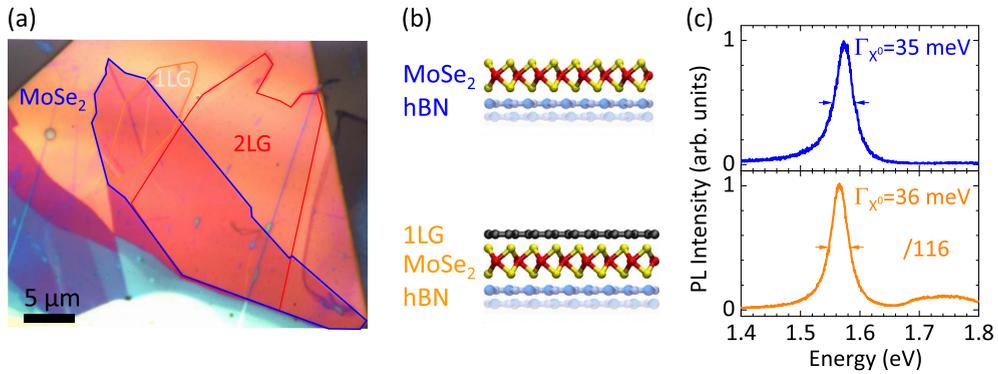
Figure 1. (a) Optical image of a hBN-supported $MoSe_2$/graphene heterostructure deposited onto an Si/SiO_2 substrate. Three regions are contoured and correspond to hBN/$MoSe_2$ (blue), hBN/$MoSe2_2$/1LG (orange) and hBN/$MoSe_2$/2LG (red). (b) Sketch of the heterostructure showing the bare $MoSe_2$ (top) and the $MoSe_2$/1LG (bottom). (c) Room Temperature photoluminescence spectra recorded on bare $MoSe_2$ (top) and $MoSe_2$/1LG (bottom). The full-width at half maximum Γ_{X^0} of the main excitonic line is indicated. Both spectra are normalized to a common value and the scaling factor between the two spectra allowing an estimation of the room temperature PL quenching factor is indicated in the lower panel. The laser wavelength is 532 nm and the laser intensity used in this experiment is near 1 $\mu W/\mu m^2$.

Indeed, the presence of charge carriers in 1LG leads to well-documented changes in the frequency (ω_G), full-width at half maximum (FWHM, Γ_G) and intensity of its one-phonon G-mode (near 1582 cm^{-1}) due to the non-adiabatic renormalization of the Kohn anomaly at the Γ point. Under moderate doping below 10^{13} cm^{-2}, this effect leads to an electron–hole symmetric upshift of ω_G accompanied by a reduction of Γ_G arising from the suppression of Landau damping [43–45]. Similar, albeit less prominent effects are also observable in 2LG [46]. Contributions from doping can be disentangled from other perturbations, in particular due to built-in or applied strain, by inspecting the correlation between ω_G and the frequency ω_{2D} of the 2D mode (near 2690 cm^{-1}, involving a pair of near-zone edge phonons with opposite momenta [42]). The slope $\partial\omega_{2D}/\partial\omega_G$ is near 2.2 under biaxial strain, directly reflecting the values of the Grüneisen parameters 2D- and G-mode phonons [47–49] but is significantly smaller than 1 in the case of hole or electron doping (Figure 2(a)) because the 2D-mode phonons have momenta significantly away from the Kohn anomaly at the zone edge (K and K′ points) [45,50].

Figure 2(a) shows the correlation between ω_G and ω_{2D} extracted from a Raman map of the monolayer $MoSe_2$/1LG area of our sample (see Figure 1(a)). Clearly, ω_{2D} and ω_G follow a linear correlation with a slope near 2.2 (Figure 2(a)), suggesting native compressive strain (i.e., stiffening of the Raman modes compared to the undoped/unstrained reference indicated in Figure 2(a)) and ruling out sizable spatially inhomogeneous residual doping. The native strain level can be as large as 0.05% (if one assumes biaxial strain [49]) and the existence of a strain gradient likely arises from the stacking process. Figure 2(b) shows the evolution of the Raman spectra as a function of the incident laser intensity from 10 $\mu W/\mu m^2$ up to 1 $mW/\mu m^2$. We observe that ω_G does not change appreciably and instead remains at 1582.2 ± 0.5 cm^{-1}. Similarly, Γ_G remains constant around $\approx$14 ± 1 cm^{-1} as it can be seen in Figure 2(c). These values are typical for quasi-neutral graphene with a residual charge density of at most a few 10^{11} cm^{-2} [45]. Hence, our observations strongly support the hypothesis that the hBN flake shields the heterostructure
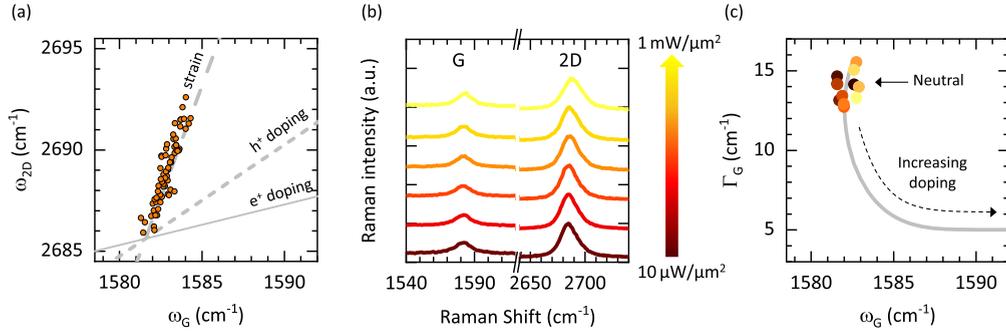
Figure 2. (a) Correlation between ω_{2D} and ω_G extracted from a Raman map of the region boxed in Figure 1(a). The dashed, short-dashed and solid gray lines indicate the correlations expected under biaxial strain, hole and electron doping, respectively. These lines cross at $(1582, 2686)$ cm^{-1}, a point that corresponds to undoped graphene with a minimal amount of built-in compressive strain below 10^{-4}. Our measurements line up on the strain line, demonstrating the existence of compressive strain gradient on the graphene layer. (b) Typical Raman spectra taken with increasing, color coded, incident laser intensity. (c) Correlation between Γ_G and ω_G under increasing incident laser intensity (color coded symbols, as in (b)). The solid gray line is the theoretically predicted correlation expected in the presence of doping using the model in Ref. [43]. All measurements were performed in ambient conditions under laser excitation at 532 nm.

from substrate-induced electron redistribution and photo-doping, yielding a pristine system to investigate exciton dynamics.

3. Low temperature hyperspectral PL mapping

Figure 3(a) shows typical low temperature (14 K) PL spectra recorded on selected spots of our sample indicated in the PL intensity map shown in Figure 3(b). An hyperspectral PL mapping study is shown in Figure 3(c)–(g). On the MoSe$_2$/hBN area, the PL spectrum is dominated by two main peaks located at 1.645 ± 0.002 eV and 1.616 ± 0.003 eV (Figure 3(c, d)). These peaks have Voigt profiles and originate from the recombination of the neutral exciton (X^0) and the trion (X*), respectively [38]. In contrast, in the 1LG and 2LG-capped MoSe$_2$ regions, the PL spectra display single, narrower quasi-Lorentzian emission lines (Figure 3(c, e)). As shown in Figure 3(a, c, d), these peaks are located at 1.636 ± 0.002 eV for hBN/MoSe$_2$/1LG and 1.633 ± 0.003 eV for hBN/MoSe$_2$/2LG, respectively. These values are slightly redshifted by 9 and 12 meV with respect to the bare MoSe$_2$ reference, respectively, due to dielectric screening [17, 51].

Considering the simplicity of the PL-spectrum of bright TMDs such as MoSe$_2$ [3,38], the single-line character of the MoSe$_2$/graphene PL spectra is essentially a consequence of the complete neutralization of the MoSe$_2$ monolayer. As confirmed by Figure 3(a, f), the integrated PL intensity near the expected location of the X* feature is vanishingly small compared to that of X^0 line (I_{X^0}) over all the 1LG and 2LG-capped MoSe$_2$ area.

The observed PL quenching, however, is a consequence of non-radiative energy transfer to graphene, stemming predominantly from hot excitons (either finite momentum X^0 excitons residing outside the light cone or excitons occupying higher-order optically active states), with a smaller contribution from cold X^0 excitons in the light cone [22]. As a result, the selected PL spectra in Figure 3(a) and total PL intensity map (I_{tot}, Figure 3(b)) reveal sizeable reduction of I_{tot} on the MoSe$_2$/1LG and MoSe$_2$/2LG regions. However, if we consider the quenching factor of the
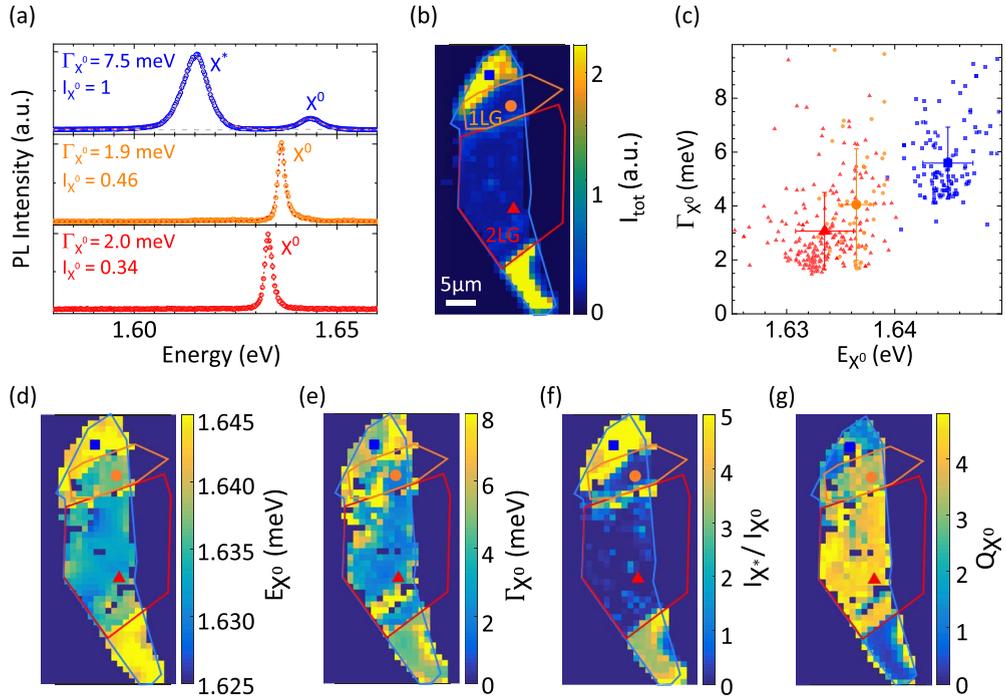
Figure 3. Low-temperature photoluminescence of the $MoSe_2$/graphene van der Waals heterostructure shown in Figure 1(a). (a) From top to bottom, selected PL spectra taken in hBN-supported $MoSe_2$ (blue), $MoSe_2$/1LG (orange) and $MoSe_2$/2LG (red) at spots indicated in the PL intensity map shown in (b). Dashed red lines in (a) are Lorentzian fits to the data (filled circles). The integrated intensity of the X^0 line is indicated in each case. Blue, orange and red contours in (b), (also in d–g) indicate the $MoSe_2$, 1LG and 2LG flakes, respectively. (c) Correlation between Γ_{X^0} and E_{X^0} extracted from the hyperspectral maps of the (d) neutral exciton emission energy E_{X^0}, (e) full-width at half maximum Γ_{X^0}, extracted from Voigt (bare $MoSe_2$) and Lorentzian ($MoSe_2$/1LG and $MoSe_2$/2LG) fits. The average values in each zone are shown with their respective standard deviations following the color code in (a, b). (f) Map of the trion-to-exciton integrated intensity ratio I_{X^*}/I_{X^0}. (g) Map of the PL quenching factor of the X^0 line. This factor, denoted Q_{X^0}, is defined relative to the spatially averaged value of I_{X^0} over the $MoSe_2$ flake shown on the lower part of the map. The data in this figure were recorded at 14 K under continuous wave laser illumination at 633 nm with a laser intensity near 100 $\mu W/\mu m^2$.

neutral exciton line X^0 only (denoted Q_{X^0}, see Figure 3(g)), we observe a moderate $Q_{X^0} = 3.3 \pm 1$ on $MoSe_2$/1LG and a slightly larger value of 4.4 ± 1 in the $MoSe_2$/2LG, in qualitative agreement with previous studies of energy transfer from individual emitters to mono and few-layer graphene [52]. The reduced quenching efficiency compared to the massive quenching observed at room temperature stems from the picosecond X^0 radiative lifetime at low temperatures [20, 21], which is comparable to the energy transfer time to graphene (see Ref. [22] for details).

Our spatially-resolved PL study also reveals narrow X^0 lines with spatially averaged FWHM (Γ_{X^0}) of 4 ± 2 meV and 3 ± 1 meV, on the $MoSe_2$/1LG and $MoSe_2$/2LG areas, respectively (Figure 3(c, e)). Interestingly, Γ_{X^0} gets as narrow as 1.6 meV in selected locations (see Figure 3(e)), a value that, even if it exceeds the homogeneous limit (0.3 meV for an estimated X^0 lifetime of 2 ps)
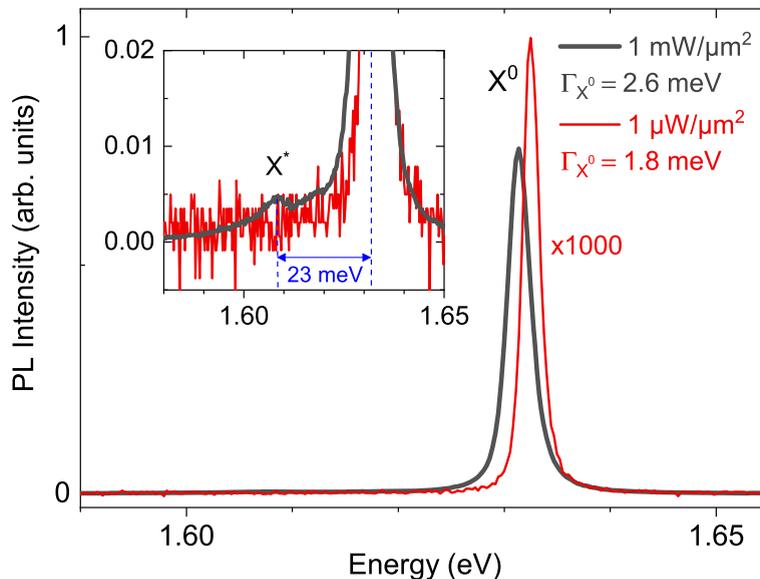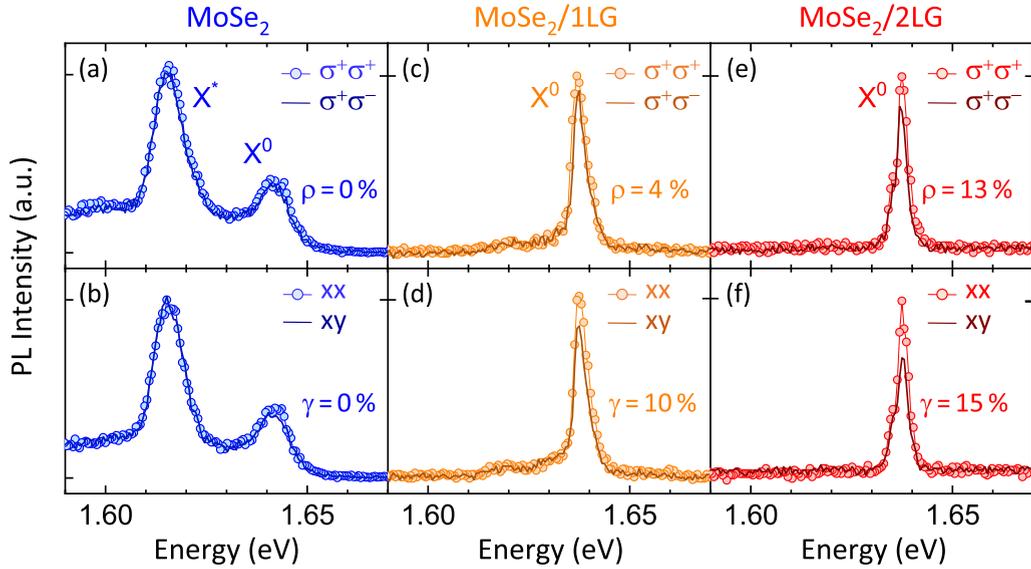
Figure 4. Photoluminescence spectra of $hBN/MoSe_2/2LG$ recorded under low and high laser intensity, near 1 $\mu W/\mu m^2$ and 1 $mW/\mu m^2$ in red and grey, respectively. Both spectra were recorded under cw excitation at 633 nm with the same integration time. The low intensity spectrum has been multiplied by a factor of 1000 for comparison. A fit of the data reveals linewidths (FWHM) of $\Gamma_{X^0} = 1.8$ and 2.6 meV at low and high intensity, respectively and an integrated intensity ratio of the exciton line very near 1000, warranting that the sample remains in the linear regime under intense cw excitation. The inset shows the low energy side of the spectra and evidences a faint feature assigned to a photoinduced trion X^* (see Ref. [22] for details). The data were recorded under cw excitation at 633 nm.

suggests that our simple sample architecture warrants reduced inhomogeneous broadening and dephasing, with values that are close to state of the art hBN-encapsulated $MoSe_2$ samples [21,35]. Figure 3(c) presents the correlation between Γ_{X^0} and E_{X^0} in each region of the sample, extracted from the maps in Figure 3(d, e). As expected, the presence of a second graphene layer improves capping and further screens the $MoSe_2$ excitons.

Let us note that although our sample is spatially homogeneous over domains as large as 50 μm^2, we observe more scattered E_{X^0}, larger Γ_{X^0} and residual trion emission (Figure 3(d–g)) near the boundaries of the 1LG and 2LG domains and also near localized micro-sized spots of our sample. During the stacking process, organic residues tend to segregate and form bubbles which locally decouple the TMD and graphene layers leading to complex spectra that reflect spatial inhomogeneities.

To close this section, let us comment on photoinduced doping at low-temperature. As indicated in Ref. [22], TMD/graphene heterostructures are extremely photostable, in stark contrast with bare TMD monolayers. By illuminating our $hBN/MoSe_2/2LG$ sample at high laser intensity (~1 $mW/\mu m^2$), a dim photo-induced trion feature with a reduced binding energy of 23 meV emerges, with an integrated intensity nearly three orders of magnitude smaller than that of the X^0 line (Figure 4). These results indicate that the $MoSe_2$ layer coupled to graphene remains essentially neutral under intense cw illumination, and that one can safely neglect photo-induced doping, including at cryogenic temperatures.

Figure 5. Low-temperature polarization-resolved photoluminescence spectra in hBN-supported MoSe$_2$ (a, b), and MoSe$_2$/1LG (c, d) and MoSe$_2$/2LG (e, f). Measurements were taken at 9 K and under optical excitation at 60 meV above the X^0 line with both circularly ($\sigma^{\pm}$) and linearly (x, y,) polarized laser excitation. Spectra in solid lines (resp. thin solid lines + symbols) correspond to cross-polarized (resp. co-polarized) incoming and emitted photons. The associated degrees of linear polarization (ρ, corresponding to the degree of valley polarization, in a, c, e) and circular polarization (γ, corresponding to the degree of valley coherence, in b, d, f) are indicated. The laser intensity is near 50 µW/µm^2 and we have verified that all regions of the sample were excited in the linear regime. The spectra are normalized for clarity and the quenching factors of the X^0 line are $Q_{X^0} = 1.8 \pm 0.1$ and 2.0 ± 0.1, respectively.

4. Valley polarization and valley coherence

We finally address the valley contrasting properties of our sample. TMD/graphene heterostructures have recently been introduced as chiral emitters with large degrees of valley polarization (ρ) and coherence (γ) up to room-temperature. Indeed, picosecond energy transfer between TMD and graphene allows the excitonic population to recombine before undergoing intervalley scattering and dephasing processes [15,53]. In addition, graphene, as a capping material, reduces disorder, spatial inhomogeneities and dephasing, which explains the large room temperature value of $\gamma \approx 20\%$ recently reported in hBN-encapsulated WS$_2$/1LG heterostructures [15]. Although improved valley contrasts come at the expense of strong PL quenching at room temperature, we expect, in keeping with the discussion above, that sizeable values of ρ and γ combined with large X^0 emission yields can be achieved at lower temperatures.

Figure 5 shows polarization-resolved PL spectra recorded using a circular and a linear basis, as well as the associated degrees of circular and linear polarization, which are directly yielding ρ and γ, respectively. For the X^0 emission line, we get $\rho \approx 0\%$, $4 \pm 4\%$ and $13 \pm 3\%$ and $\gamma \approx 0\%$, $10 \pm 5\%$ and $15 \pm 4\%$ for hBN-supported MoSe$_2$, MoSe$_2$/1LG and MoSe$_2$/2LG, respectively.

Near-zero values of ρ have been reported in MoSe$_2$ monolayers [36]. Since the low temperature X^0 lifetimes in bare MoSe$_2$ and in MoSe$_2$/graphene heterostructures are similar [21,22], the observation of modest values of ρ in MoSe$_2$/graphene is not surprising. Noteworthy, γ signifi-

cantly exceeds ρ in MoSe$_2$/1LG and MoSe$_2$/2LG, suggesting significantly reduced dephasing in encapsulated samples, as recently observed in MoS$_2$ monolayers fully encapsulated in hBN [31] and in hBN-capped WS$_2$/1LG [15]. Here, our measurements are performed at 60 meV above the X^0 line. We anticipate larger values of ρ and γ as we excite MoSe$_2$/graphene samples closer to the X^0 resonance. In addition, one may also optimize the sample geometry as in Refs [21,35] in order to minimize the radiative lifetime of the MoSe$_2$ monolayer, and hence optimize ρ and γ.

5. Conclusion and perspectives

We have demonstrated that hBN-supported TMD/graphene heterostructures offer an excellent template to study electron redistribution and excitonic energy transfer in two dimensions, with donor–acceptor distances in the sub-nanometer range. The absence of photodoping in hBN-supported samples as compared to SiO$_2$-supported systems adds on to the merits of hBN as an ideal dielectrics for van der Waals assembly. Our study also establishes that bright TMD emission with linewidths approaching the homogenous limit can be achieved over large areas using only one epilayer of graphene, hence without the need of an hBN capping layer. In this manner, one does not only benefit from the emission filtering properties of graphene but also from its assets as a capping van der Waals material.

In spite of recent advances [17–19, 22, 54] the microscopic details of the transfer mechanism are still under investigation. Focusing for instance on energy transfer, Dexter- and Förster-type mechanisms depend sensitively on the distance between the layers and on the local environment. Investigations of the transfer efficiency while finely tuning the TMD-graphene distance using hBN spacers and as a function of the number of graphene layers should bring decisive insights into near-field coupling in van der Waals materials.

Our work also holds promise for device-oriented research. Indeed, the absence of a top hBN layer allows us to directly contact the graphene electrode for photodetectors and light-emitting devices, as well as for local investigations, e.g., using scanning tunnelling microscopy [55]. Conversely, TMDs have recently been shown to outperform hBN as a capping material, yielding record-high room temperature electron mobility in graphene [56].

Finally, a challenging yet appealing perspective would consist in exploiting low-energy surface plasmon polaritons in graphene to tailor light-matter interactions in near-field coupled two-dimensional semiconductors [57], including in quantum wells made from the latter [58].

6. Experimental details

Our van der Waals heterstructure was prepared using standard micromechanical exfoliation and dry transfer methods, as in Ref. [59]. The hBN flake was mechanically exfoliated on top of the substrate. A MoSe$_2$ monolayer and a single- and bilayer graphene flake were mechanically exfoliated from bulk crystals and then stacked on top of the hBN flake. The number of layers of the flakes were verified using room-temperature Raman and PL spectroscopy. PL and Raman scattering measurements in Figures 1 and 2, respectively, were performed in ambient air using a 532 nm diode pumped solid state laser and a home-built scanning confocal setup. Low temperature PL studies were performed in a continuous-flow liquid helium cryostat mounted onto our Raman/PL microscope. All PL measurements in Figure 3 were recorded in the linear regime under cw excitation at 633 nm, i.e., slightly above the B exciton in MoSe$_2$ [3, 17]. The low-temperature polarization-resolved measurements in Figure 5 were performed under near-resonant optical excitation 60 meV above the neutral exciton (X^0) line using a tunable supercontinuum laser. The degree of valley polarization $\rho = (I_{\sigma^+\sigma^+} - I_{\sigma^+\sigma^-})/(I_{\sigma^+\sigma^+} + I_{\sigma^+\sigma^-})$ is measured in a circular basis and the degree of valley coherence $\gamma = (I_{xx} - I_{xy})/(I_{xx} + I_{xy})$ is measured in a linear basis.

In these expressions, I_{ij} indicates the PL intensity detected in the "i" polarization state when upon excitation under "j" polarized light ($i, j = \sigma^{\pm}$ or x/y). A Linear polarizer and an achromatic quarter-waveplate were used to prepare the polarization state of the incoming beam. The emitted photons propagate through the same quarter-wave plate and are analyzed using a Wollaston prism, which permits to record simultaneously the co- and cross polarized PL signals. The values of ρ and γ were determined from fits of the X^0 lines.

Acknowledgements

References

[1] K. F. Mak, C. Lee, J. Hone, J. Shan, T. F. Heinz, "Atomically thin MoS$_2$: a new direct-gap semiconductor", *Phys. Rev. Lett.* **105** (2010), no. 13, article no. 136805.

[2] A. Splendiani, L. Sun, Y. Zhang, T. Li, J. Kim, C.-Y. Chim, G. Galli, F. Wang, "Emerging photoluminescence in monolayer MoS$_2$", *Nano Lett.* **10** (2010), no. 4, p. 1271-1275.

[3] G. Wang, A. Chernikov, M. M. Glazov, T. F. Heinz, X. Marie, T. Amand, B. Urbaszek, "Colloquium: excitons in atomically thin transition metal dichalcogenides", *Rev. Mod. Phys.* **90** (2018), article no. 021001.

[4] M. Goryca, J. Li, A. V. Stier, T. Taniguchi, K. Watanabe, E. Courtade, S. Shree, C. Robert, B. Urbaszek, X. Marie, S. A. Crooker, "Revealing exciton masses and dielectric properties of monolayer semiconductors with high magnetic fields", *Nat. Commun.* **10** (2019), no. 1, article no. 4172.

[5] X. Xu, W. Yao, D. Xiao, T. F. Heinz, "Spin and pseudospins in layered transition metal dichalcogenides", *Nat. Phys.* **10** (2014), no. 5, p. 343-350.

[6] J. R. Schaibley, H. Yu, G. Clark, P. Rivera, J. S. Ross, K. L. Seyler, W. Yao, X. Xu, "Valleytronics in 2D materials", *Nat. Rev. Mater.* **1** (2016), article no. 16055.

[7] K. F. Mak, J. Shan, "Photonics and optoelectronics of 2D semiconductor transition metal dichalcogenides", *Nat. Photonics* **10** (2016), no. 4, p. 216-226.

[8] L. Ciorciaro, M. Kroner, K. Watanabe, T. Taniguchi, A. Imamoglu, "Observation of magnetic proximity effect using resonant optical spectroscopy of an electrically tunable MoSe$_2$/CrBr$_3$ heterostructure", *Phys. Rev. Lett.* **124** (2020), article no. 197401.

[9] T. P. Lyons, D. Gillard, A. Molina-Sánchez, A. Misra, F. Withers, P. S. Keatley, A. Kozikov, T. Taniguchi, K. Watanabe, K. S. Novoselov, J. Fernández-Rossier, A. I. Tartakovskii, "Interplay between spin proximity effect and charge-dependent exciton dynamics in MoSe2/CrBr3 van der Waals heterostructures", *Nat. Commun.* **11** (2020), no. 1, article no. 6021.

[10] M. Massicotte, P. Schmidt, F. Vialla, K. Schädler, A. Reserbat-Plantey, K. Watanabe, T. Taniguchi, K. Tielrooij, F. Koppens, "Picosecond photoresponse in van der Waals heterostructures", *Nat. Nanotechnol.* **11** (2016), no. 1, p. 42-46.

[11] Y. K. Luo, J. Xu, T. Zhu, G. Wu, E. J. McCormick, W. Zhan, M. R. Neupane, R. K. Kawakami, "Opto-valleytronic spin injection in monolayer MoS$_2$/few-layer graphene hybrid spin valves", *Nano Lett.* **17** (2017), no. 6, p. 3877-3883.

[12] A. Avsar, D. Unuchek, J. Liu, O. L. Sanchez, K. Watanabe, T. Taniguchi, B. Özyilmaz, A. Kis, "Optospintronics in graphene via proximity coupling", *ACS Nano* **11** (2017), no. 11, p. 11678-11686.

[13] A. H. Castro Neto, F. Guinea, N. M. R. Peres, K. S. Novoselov, A. K. Geim, "The electronic properties of graphene", *Rev. Mod. Phys.* **81** (2009), p. 109-162.

[14] K. F. Mak, L. Ju, F. Wang, T. F. Heinz, "Optical spectroscopy of graphene: from the far infrared to the ultraviolet", *Solid State Commun.* **152** (2012), no. 15, p. 1341-1349.

[15] E. Lorchat, S. Azzini, T. Chervy, T. Taniguchi, K. Watanabe, T. W. Ebbesen, C. Genet, S. Berciaud, "Room-temperature valley polarization and coherence in transition metal dichalcogenide–graphene van der waals heterostructures", *ACS Photonics* **5** (2018), no. 12, p. 5047-5054.

[16] J. He, N. Kumar, M. Z. Bellus, H.-Y. Chiu, D. He, Y. Wang, H. Zhao, "Electron transfer and coupling in graphene–tungsten disulfide van der Waals heterostructures", *Nat. Commun.* **5** (2014), article no. 5622.

[17] G. Froehlicher, E. Lorchat, S. Berciaud, "Charge versus energy transfer in atomically thin graphene-transition metal dichalcogenide van der Waals heterostructures", *Phys. Rev. X* **8** (2018), article no. 011007.

[18] L. Yuan, T.-F. Chung, A. Kuc, Y. Wan, Y. Xu, Y. P. Chen, T. Heine, L. Huang, "Photocarrier generation from interlayer charge-transfer transitions in WS_2-graphene heterostructures", *Sci. Adv.* **4** (2018), no. 2, article no. e1700324.

[19] M. Selig, E. Malic, K. J. Ahn, N. Koch, A. Knorr, "Theory of optically induced Förster coupling in van der Waals coupled heterostructures", *Phys. Rev. B* **99** (2019), article no. 035420.

[20] C. Robert, D. Lagarde, F. Cadiz, G. Wang, B. Lassagne, T. Amand, A. Balocchi, P. Renucci, S. Tongay, B. Urbaszek, X. Marie, "Exciton radiative lifetime in transition metal dichalcogenide monolayers", *Phys. Rev. B* **93** (2016), article no. 205423.

[21] H. H. Fang, B. Han, C. Robert, M. A. Semina, D. Lagarde, E. Courtade, T. Taniguchi, K. Watanabe, T. Amand, B. Urbaszek, M. M. Glazov, X. Marie, "Control of the exciton radiative lifetime in van der Waals heterostructures", *Phys. Rev. Lett.* **123** (2019), article no. 067401.

[22] E. Lorchat, L. E. P. López, C. Robert, D. Lagarde, G. Froehlicher, T. Taniguchi, K. Watanabe, X. Marie, S. Berciaud, "Filtering the photoluminescence spectra of atomically thin semiconductors with graphene", *Nat. Nanotechnol.* **15** (2020), no. 4, p. 283-288.

[23] Y.-J. Yu, Y. Zhao, S. Ryu, L. E. Brus, K. S. Kim, P. Kim, "Tuning the graphene work function by electric field effect", *Nano Lett.* **9** (2009), no. 10, p. 3430-3434.

[24] Y. Liang, S. Huang, R. Soklaski, L. Yang, "Quasiparticle band-edge energy and band offsets of monolayer of molybdenum and tungsten chalcogenides", *Appl. Phys. Lett.* **103** (2013), no. 4, article no. 042106.

[25] N. R. Wilson, P. V. Nguyen, K. Seyler, P. Rivera, A. J. Marsden, Z. P. L. Laker, G. C. Constantinescu, V. Kandyba, A. Barinov, N. D. M. Hine, X. Xu, D. H. Cobden, "Determination of band offsets, hybridization, and exciton binding in 2D semiconductor heterostructures", *Sci. Adv.* **3** (2017), no. 2, article no. e1601832.

[26] H. M. Hill, A. F. Rigosi, A. Raja, A. Chernikov, C. Roquelet, T. F. Heinz, "Exciton broadening in WS_2/graphene heterostructures", *Phys. Rev. B* **96** (2017), article no. 205401.

[27] S. Ryu, L. Liu, S. Berciaud, Y.-J. Yu, H. Liu, P. Kim, G. W. Flynn, L. E. Brus, "Atmospheric oxygen binding and hole doping in deformed graphene on a SiO_2 substrate", *Nano Lett.* **10** (2010), no. 12, p. 4944-4951.

[28] B. Miller, E. Parzinger, A. Vernickel, A. W. Holleitner, U. Wurstbauer, "Photogating of mono-and few-layer MoS_2", *Appl. Phys. Lett.* **106** (2015), no. 12, article no. 122103.

[29] W. Lin, P. Zhuang, H. Chou, Y. Gu, R. Roberts, W. Li, S. K. Banerjee, W. Cai, D. Akinwande, "Electron redistribution and energy transfer in graphene/MoS2 heterostructure", *Appl. Phys. Lett.* **114** (2019), no. 11, article no. 113103.

[30] C. R. Dean, A. F. Young, I. Meric, C. Lee, L. Wang, S. Sorgenfrei, K. Watanabe, T. Taniguchi, P. Kim, K. Shepard *et al.*, "Boron nitride substrates for high-quality graphene electronics", *Nat. Nanotechnol.* **5** (2010), no. 10, p. 722-726.

[31] F. Cadiz, E. Courtade, C. Robert, G. Wang, Y. Shen, H. Cai, T. Taniguchi, K. Watanabe, H. Carrere, D. Lagarde, M. Manca, T. Amand, P. Renucci, S. Tongay, X. Marie, B. Urbaszek, "Excitonic linewidth approaching the homogeneous limit in MoS_2-based van der Waals heterostructures", *Phys. Rev. X* **7** (2017), article no. 021026.

[32] O. A. Ajayi, J. V. Ardelean, G. D. Shepard, J. Wang, A. Antony, T. Taniguchi, K. Watanabe, T. F. Heinz, S. Strauf, X.-Y. Zhu, J. C. Hone, "Approaching the intrinsic photoluminescence linewidth in transition metal dichalcogenide monolayers", *2D Mater.* **4** (2017), no. 3, article no. 031011.

[33] P. Back, S. Zeytinoglu, A. Ijaz, M. Kroner, A. Imamoğlu, "Realization of an electrically tunable narrow-bandwidth atomically thin mirror using monolayer $MoSe_2$", *Phys. Rev. Lett.* **120** (2018), article no. 037401.

[34] G. Scuri, Y. Zhou, A. A. High, D. S. Wild, C. Shu, K. De Greve, L. A. Jauregui, T. Taniguchi, K. Watanabe, P. Kim, M. D. Lukin, H. Park, "Large excitonic reflectivity of monolayer $MoSe_2$ encapsulated in hexagonal boron nitride", *Phys. Rev. Lett.* **120** (2018), article no. 037402.

[35] Y. Zhou, G. Scuri, J. Sung, R. J. Gelly, D. S. Wild, K. De Greve, A. Y. Joe, T. Taniguchi, K. Watanabe, P. Kim, M. D. Lukin, H. Park, "Controlling excitons in an atomically thin membrane with a mirror", *Phys. Rev. Lett.* **124** (2020), article no. 027401.

[36] G. Wang, E. Palleau, T. Amand, S. Tongay, X. Marie, B. Urbaszek, "Polarization and time-resolved photoluminescence spectroscopy of excitons in $MoSe_2$ monolayers", *Appl. Phys. Lett.* **106** (2015), no. 11, article no. 112101.

[37] G. Kioseoglou, A. T. Hanbicki, M. Currie, A. L. Friedman, B. T. Jonker, "Optical polarization and intervalley scattering in single layers of MoS_2 and $MoSe_2$", *Sci. Rep.* **6** (2016), article no. 25041.

[38] J. S. Ross, S. Wu, H. Yu, N. J. Ghimire, A. M. Jones, G. Aivazian, J. Yan, D. G. Mandrus, D. Xiao, W. Yao *et al.*, "Electrical control of neutral and charged excitons in a monolayer semiconductor", *Nat. Commun.* **4** (2013), article no. 1474.

[39] S. Barja, S. Refaely-Abramson, B. Schuler, D. Y. Qiu, A. Pulkin, S. Wickenburg, H. Ryu, M. M. Ugeda, C. Kastl, C. Chen *et al.*, "Identifying substitutional oxygen as a prolific point defect in monolayer transition metal dichalcogenides", *Nat. Commun.* **10** (2019), no. 1, article no. 3382.

[40] T. Ahmed, K. Roy, S. Kakkar, A. Pradhan, A. Ghosh, "Interplay of charge transfer and disorder in optoelectronic response in Graphene/hBN/MoS2 van der Waals heterostructures", *2D Mater.* **7** (2020), article no. 025043.

[41] W. Zhang, C.-P. Chuu, J.-K. Huang, C.-H. Chen, M.-L. Tsai, Y.-H. Chang, C.-T. Liang, Y.-Z. Chen, Y.-L. Chueh, J.-H. He, M.-Y. Chou, L.-J. Li, "Ultrahigh-gain photodetectors based on atomically thin graphene-MoS$_2$ heterostructures", *Sci. Rep.* **4** (2014), article no. 3826.

[42] A. C. Ferrari, D. M. Basko, "Raman spectroscopy as a versatile tool for studying the properties of graphene", *Nat. Nanotechnol.* **8** (2013), no. 4, p. 235-246.

[43] S. Pisana, M. Lazzeri, C. Casiraghi, K. S. Novoselov, A. K. Geim, A. C. Ferrari, F. Mauri, "Breakdown of the adiabatic Born-Oppenheimer approximation in graphene", *Nat. Mater.* **6** (2007), no. 3, p. 198-201.

[44] J. Yan, Y. Zhang, P. Kim, A. Pinczuk, "Electric field effect tuning of electron-phonon coupling in graphene", *Phys. Rev. Lett.* **98** (2007), no. 16, article no. 166802.

[45] G. Froehlicher, S. Berciaud, "Raman spectroscopy of electrochemically gated graphene transistors: geometrical capacitance, electron-phonon, electron-electron, and electron-defect scattering", *Phys. Rev. B* **91** (2015), article no. 205413.

[46] J. Yan, E. Henriksen, P. Kim, A. Pinczuk, "Observation of anomalous phonon softening in bilayer graphene", *Phys. Rev. Lett.* **101** (2008), article no. 136804.

[47] J. E. Lee, G. Ahn, J. Shim, Y. S. Lee, S. Ryu, "Optical separation of mechanical strain from charge doping in graphene", *Nat. Commun.* **3** (2012), article no. 1024.

[48] D. Metten, F. Federspiel, M. Romeo, S. Berciaud, "Probing built-in strain in freestanding graphene monolayers by Raman spectroscopy", *Phys. Status Solidi (b)* **250** (2013), no. 12, p. 2681-2686.

[49] D. Metten, F. Federspiel, M. Romeo, S. Berciaud, "All-optical blister test of suspended graphene using micro-Raman spectroscopy", *Phys. Rev. Appl.* **2** (2014), article no. 054008.

[50] A. Das, S. Pisana, B. Chakraborty, S. Piscanec, S. K. Saha, U. V. Waghmare, K. S. Novoselov, H. R. Krishnamurthy, A. K. Geim, A. C. Ferrari, A. K. Sood, "Monitoring dopants by Raman scattering in an electrochemically top-gated graphene transistor", *Nat. Nanotechnol.* **3** (2008), no. 4, p. 210-215.

[51] A. Raja, A. Chaves, J. Yu, G. Arefe, H. M. Hill, A. F. Rigosi, T. C. Berkelbach, P. Nagler, C. Schüller, T. Korn, C. Nuckolls, J. Hone, L. E. Brus, T. F. Heinz, D. R. Reichman, A. Chernikov, "Coulomb engineering of the bandgap and excitons in two-dimensional materials", *Nat. Commun.* **8** (2017), article no. 15251.

[52] Z. Chen, S. Berciaud, C. Nuckolls, T. F. Heinz, L. E. Brus, "Energy transfer from individual semiconductor nanocrystals to graphene", *ACS Nano* **4** (2010), no. 5, p. 2964-2968.

[53] I. Paradisanos, K. M. McCreary, D. Adinehloo, L. Mouchliadis, J. T. Robinson, H.-J. Chuang, A. T. Hanbicki, V. Pere-beinos, B. T. Jonker, E. Stratakis, G. Kioseoglou, "Prominent room temperature valley polarization in WS2/graphene heterostructures grown by chemical vapor deposition", *Appl. Phys. Lett.* **116** (2020), no. 20, article no. 203102.

[54] S. Aeschlimann, A. Rossi, M. Chávez-Cervantes, R. Krause, B. Arnoldi, B. Stadtmüller, M. Aeschlimann, S. Forti, F. Fabbri, C. Coletti, I. Gierz, "Direct evidence for efficient ultrafast charge separation in epitaxial WS2/graphene heterostructures", *Sci. Adv.* **6** (2020), no. 20, article no. eaay0761.

[55] D. Pommier, R. Bretel, L. E. P. López, F. Fabre, A. Mayne, E. Boer-Duchemin, G. Dujardin, G. Schull, S. Berciaud, E. Le Moal, "Scanning tunneling microscope-induced excitonic luminescence of a two-dimensional semiconductor", *Phys. Rev. Lett.* **123** (2019), article no. 027402.

[56] L. Banszerus, T. Sohier, A. Epping, F. Winkler, F. Libisch, F. Haupt, K. Watanabe, T. Taniguchi, K. Müller-Caspary, N. Marzari *et al.*, "Extraordinary high room-temperature carrier mobility in graphene-WSe$_2$ heterostructures", https://arxiv.org/abs/1909.09523, 2019.

[57] Y. Kurman, N. Rivera, T. Christensen, S. Tsesses, M. Orenstein, M. Soljačić, J. D. Joannopoulos, I. Kaminer, "Control of semiconductor emitter frequency by increasing polariton momenta", *Nat. Photonics* **12** (2018), no. 7, p. 423-429.

[58] P. Schmidt, F. Vialla, S. Latini, M. Massicotte, K.-J. Tielrooij, S. Mastel, G. Navickaite, M. Danovich, D. A. Ruiz-Tijerina, C. Yelgel, V. Fal'ko, K. S. Thygesen, R. Hillenbrand, F. H. L. Koppens, "Nano-imaging of intersubband transitions in van der Waals quantum wells", *Nat. Nanotechnol.* **13** (2018), no. 11, p. 1035-1041.

[59] A. Castellanos-Gomez, M. Buscema, R. Molenaar, V. Singh, L. Janssen, H. S. J. van der Zant, G. A. Steele, "Deterministic transfer of two-dimensional materials by all-dry viscoelastic stamping", *2D Mater.* **1** (2014), article no. 011002.